Bull. Astr. Soc. India (1990) **18**, 17-32

Effects of dust on equivalent widths of spectral lines formed in expanding spherically symmetric shells

A. Peraiah and M. F. Ingalgi

Indian Institute of Astrophysics, Sarjapur Road, Koramangala, Bangalore 560 034

Received 1990 January 19; accepted 1990 February 10

Abstract. We have studied the effects of the presence of dust and radial expansion of the spherical shells around stars on the equivalent widths of the lines formed in such shells. We have considered a non-LTE, two level atom approximation and assumed that the dust scatters isotropically. We have considered 30 shells and an optical depth of 300. In the case of dust we have considered only dust scattering and neglected absorption due to dust ($\omega = 1$, where ω is the albedo for single scattering). We have treated two types of expanding shells (i) with velocity gradients and (ii) without velocity gradients. Depending upon the parameters we used, the equivalent widths change considerably.

Key words : radiative transfer—spectral line formation—equivalent width—dust

1. Introduction

Infrared observations reveal the presence of dust in the outermost layers of stars. Br α line radiation was observed in Beckline-Neugebauer (BN) object in Orion by Grasdalen (1976). These objects show the presence of ionized gas and several of such objects e.g. BN and CRL 490) seem to possess dusty shells around a hard core of ionized gas. Br γ, Pf γ, Br γ infrared lines have been observed in the compact molecular clouds by Simon *et al.* (1981, 1985). Persi *et al.* (1983) derived mass loss rates for 15 Of-type stars based upon infrared photometric observations from 2.3 μm to 10 μm. Infrared observations of several objects such as gaseous nebulae, active galactic nuclei, T-Tauri stars, atmospheres of cool supergiants show the presence of dust in the outer envelopes of these objects. Allen (1973) studied many early type emission line stars and found that free-free emission and thermal emission from dust grains are the sources of the infrared excesses. Geisel (1970) and Allen & Swings (1972) found that stars with prominent infrared continua appear to have circumstellar envelopes. Schwartz *et al.* (1983) studied the far-infrared and submillimeter mapping of S140 IRS and concluded that there is a good coupling between dust and gas. Huggins *et al.* (1984) derived abundances in the envelopes of

IRC + 10216 by line analysis, following the approach of Kwan & Hill (1977) and Henkel *et al.* (1983). Felli (1982) studied the infrared emission from extended stellar envelope.

The line formation calculations should include dust, radial expansion, geometrical extension of the outer shells, and chemical species. Recently, calculations have been carried out which include dust and expansion (see Peraiah & Wehrse 1978, Wehrse & Peraiah 1979, Hummer & Kunasz 1980, Wehrse & Kalkofen 1985, Peraiah *et al.* 1987).

In this paper we calculate the lines formed in the expanding extended spherical shells filled with dust and gas. We calculate the equivalent widths so that it is easy to compare with the observed lines formed in such media.

2. Calculations

We perform the calculations in a comoving frame and the equation of transfer in such a frame is written as (Peraiah *et al.* 1987, Chandrasekhar 1945, Mihalas *et al.* 1975, Mihalas 1978):

$$\mu \frac{\partial I(r, \mu, x)}{\partial r} + \frac{1-\mu^2}{r} \frac{\partial I(r, \mu, x)}{\partial \mu} = K_L(r)[\phi(x) + \beta]\,[S(r, \mu, x) - I(r, \mu, x)] + \left\{(1-\mu^2)\frac{V(r)}{r} + \mu^2 \frac{dV(r)}{dr}\right\} \times \frac{\partial I(r, \mu, x)}{\partial x} + K_{dust}(r)\{S_{dust}(r, \mu, x) - I(r, \mu, x)\}. \quad \ldots(1)$$

For the oppositely directed beam, we have

$$-\mu \frac{\partial I(r, -\mu, x)}{\partial r} + \frac{1-\mu^2}{r} \frac{\partial I(r, -\mu, x)}{\partial \mu} = K_L(r)[\phi(x) + \beta]\,[S(r, -\mu, x) - I(r, -\mu, x)] \left\{(1-\mu^2)\frac{V(r)}{r} + \mu^2 \frac{dV(r)}{dr}\right\} \times \frac{\partial I(r, -\mu, x)}{\partial x} + K_{dust}(r)\{S_{dust}(r, -\mu, x) - I(r, -\mu, x)\}. \quad \ldots(2)$$

where $\mu \in (0, 1)$. Here $K_L(r)$ is the absorption coefficient at the line centre, $\phi(x)$ the Doppler profile function, and β the ratio of continuum to line absorption coefficients. The quantity $S(r, \pm\mu, x)$ is the source function given by

$$S(r, \pm\mu, x) = \frac{\phi(x)}{\phi(x)+\beta} S_L(r) + \frac{\beta}{\phi(x)+\beta} S_c(r, x) \quad \ldots(3)$$

with

$$S_L(r) = \frac{(1-\epsilon)}{2}\int_{-\infty}^{+\infty} \phi(x) \int_{-1}^{+1} I(r, \mu', x)\, dx d\mu' + \epsilon B(T(r), x), \quad \ldots(4)$$

$$S_C(r, x) = \rho(r) B(T(r), x), \quad \ldots(5)$$

where $\rho(r)$ is an arbitrary factor.

S_L and S_C are the source functions in the line and continuum respectively. $B(T_e(r), x)$ is the Planck function.

The quantity ϵ is the probability per scatter that a photon is thermalized because of collisional de-excitation. This is given by (see Grant & Peraiah 1972)

$$\epsilon = \frac{C_{21}}{C_{21} + A_{21}[1 - \exp(-h\nu_0/kT_e]^{-1}} \quad \ldots(6)$$

where C_{21} is the collisional de-excitation rate and A_{21} the spontaneous emission rate. The quantity $I(r, \mu, x)$ is the specific intensity of the ray making an angle $\cos^{-1}\mu$ with the radius vector r at a standardized frequency x given by

$$x = (\nu - \nu_0)/\Delta, \quad \ldots(7)$$

Δ being mean thermal Doppler width. $V(r)$ is the velocity of expansion of gases in Doppler units. The line profile $\phi(x)$ is normalized such that

$$\int_{-\infty}^{+\infty} \phi(x)dx = 1, \quad \ldots(8)$$

We employed a two-level atom approximation the statistical equilibrium equation of which is given by

$$N_1\{B_{12}\int_{-\infty}^{+\infty} \phi(x)J_x dx + C_{12}\} = N_1\{B_{12}\int_{-\infty}^{+\infty} \phi(x)J_x dx + C_{12} + A_{21}\}, \quad \ldots(9)$$

where B_{12} and B_{21} are the Einstein coefficients and N_1 and N_2 are the population densities in levels 1 and 2 respectively. The quantity S_{dust} $(r, \pm\mu, x)$ is the source function due to dust and is given by

$$S_{dust}(r, \pm\mu, x) = (1 - \omega)B_{dust} + \frac{\omega}{2}\int_{-\infty}^{+\infty} P(\mu, \mu', r)I(r, \mu', x)d\mu' \quad \ldots(10)$$

where B_{dust} is the Planck function for the emission, ω is the albedo for single scattering and $P(\mu, \mu', r)$ is the phase function. We have set $\omega = 1$ (pure scattering) and employed isotropic scattering. We can safely neglect the emission from dust as it will not change the line profiles. The equivalent width is calculated by the formula

$$Eq.\ W = \int_{-\alpha}^{+\alpha}\left(1 - \frac{F_x}{F_c}\right) dx, \quad \ldots(11)$$

where α is the half band width of the line (*i.e.*) $\alpha = \max|x|$, F_c is the flux in the immediate neighbourhood continuum of the line and F_x the flux at point x. The integration of equations (1) and (2) is done according to the procedure described in Peraiah *et al.* (1987). Results are presented below.

3. Results and discussions

The aim of this paper is to investigate the effects of dust and radial expansion of the outer layers on the equivalent widths as equivalent widths indicate the total amount of absorption or emission. We have chosen trepazoidal points for frequency integration and Gauss-Legendre points for angle integration. We have employed nine frequency points ($I = 9$) with one frequency point always at the centre of the line and two angles ($m = 2$) in each half space. Therefore the working matrix of the calculation becomes (18×18). This is accurate enough to give precision permitted by the machine. We have several physical situations to study and therefore the number of parameters will be quite large and we have to restrict to physically meaningful parameters. We set the dust density and gas density constant through the medium.

Boundary condition

We assume that no radiation is incident from outside the spherical shell at $r = B$ and $\tau = 0$, while radiation of unit intensity is incident at $r = A$, $\tau = \tau_{max} = T$, in the case of a purely scattering medium. When there is emission from within the medium, no radiation is assumed to be incident at either of the two boundaries. Thus, we have

$$\left.\begin{aligned} U^{-}(\tau = T,\ \mu_j) &= 1 \\ U^{+}(\tau = 0,\ \mu_j) &= 0 \end{aligned}\right\}, (\epsilon = 0,\quad \beta = 0), \qquad \ldots(12)$$

and

$$\left.\begin{aligned} U^{-}(\tau = T,\ \mu_j) &= 0 \\ U^{+}(\tau = 0,\ \mu_j) &= 0 \end{aligned}\right\}, \quad (\epsilon > 0 \ \text{ or } \ \beta > 0). \qquad \ldots(13)$$

In the case of the boundary condition of the frequency derivative, we have

$$\frac{\partial U^{+}}{\partial X}(\text{at } X = |X_{max}|) = 0. \qquad \ldots(14)$$

We have set the velocities at $r = A$ to be V_A, and at $r = B$ as V_B. If the spherical shell expands with constant velocity, we have

$$V_A = V_B; \qquad \ldots(15)$$

and if there are velocity gradients, then

$$V_A = 0 \text{ and } V_B > 0. \qquad \ldots(16)$$

We describe the profiles in terms of the fluxes integrated over the whole disc versus the normalized frequency. The results are presented in the figures for the following parameters:

B/A = The ratio of the outer to inner radii of the spherical shell. We have set $B/A = 20$ in all cases,
ϵ = the probability per scattering that a photon is lost by collisional de-excitation,
β = the ratio of the absorption coefficient per unit frequency interval in the continuum to that at the line centre,

V_A = the velocity in Doppler units (or mtu) at the point $r = A$,
V_B = the velocity in Doppler units at the point $r = B$ in the spherical medium,
V = the velocity of expansion of the shell,
τ_d = total dust optical depth,
T = total gas optical depth at the line centre = 300.

We have divided the spherical shell into 30 shells and computed the emergent as well as the internal radiation field by using the algorithm described by Peraiah (1984).

In figures 1 to 4 the line profiles are plotted with respect to the normalized frequency X in a static medium. We have progressively increased the dust optical depth from 0 to 5. When there is no dust, the wings of the lines (shown in figure 1) are substantially higher and as the amount of dust is increased the emission in the wings falls quite rapidly. In figure 4 there is hardly any emission. When there is no dust the absorption core is very wide extending approximately to three Doppler units on either side of the centre of the line. However, when the optical depth of the dust is increased to five, the width of the absorption core reduced to only approximately 1.5 Doppler units on either side of the centre of the line. This shows that dust scatters photons mostly into the cores of the absorption lines and removes photons from the wings. In figures 5 to 8 we have given an

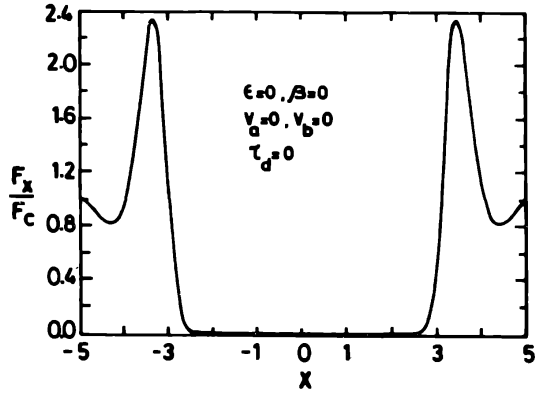

Figure 1. Line profiles formed in a static medium without dust ($\tau_d = 0$).

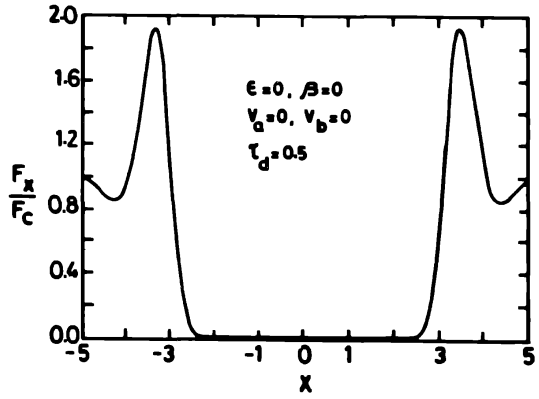

Figure 2. Same as in figure 1 for $\tau_d = 0.05$, dust being distributed uniformly.

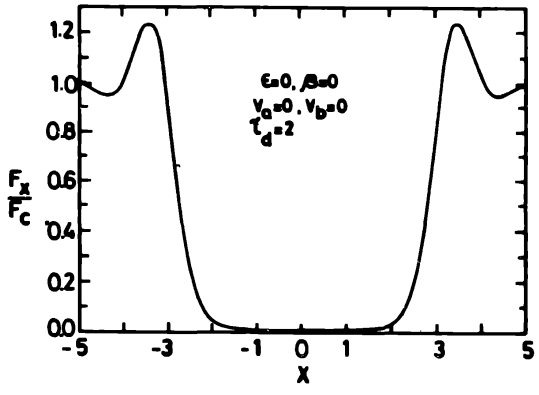

Figure 3. Same as in figure 2 with dust optical depth, $\tau_d = 2$.

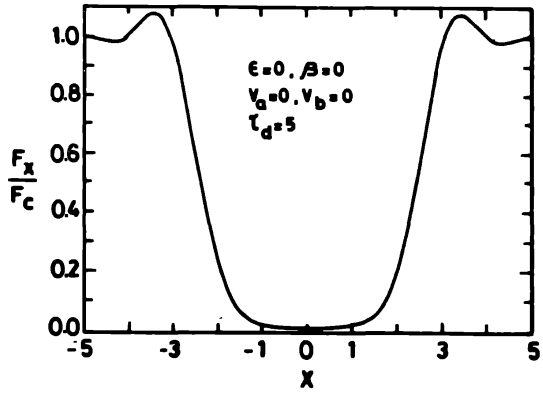

Figure 4. Same as in figure 2 with dust optical depth $\tau_d = 5$.

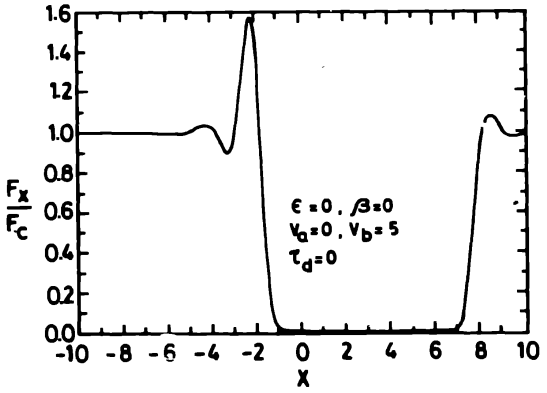

Figure 5. Line profiles formed in an expanding medium with velocity gradients and velocity of expansion $V_b = 5$ mtu and with no dust.

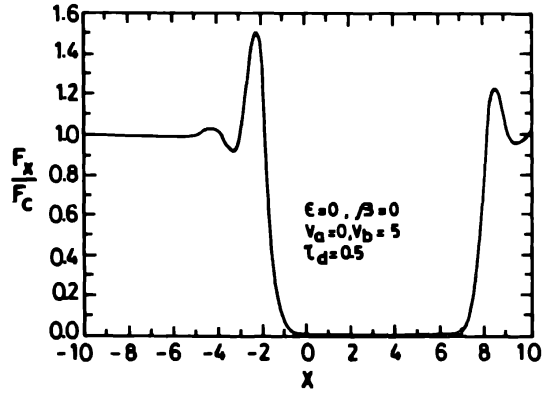

Figure 6. Same as in figure 5 with dust distributed uniformly having $\tau_d = 0.5$.

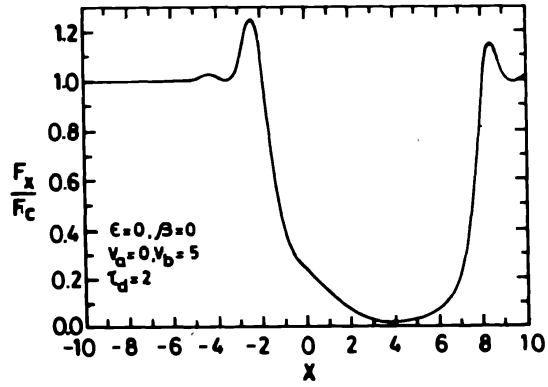

Figure 7. Same as in figure 5 with dust distributed uniformly having $\tau_d = 2$.

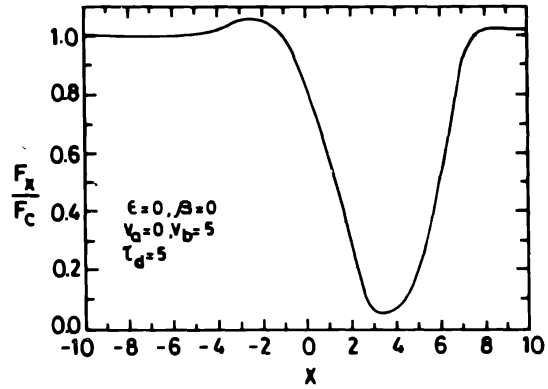

Figure 8. Same as in figure 5 with dust distributed uniformly having $\tau_d = 5$.

expansion velocity of 5 mtu again with dust optical depth progressively increasing. We see that lines have become asymmetric and the same effects as seen in figures 1 to 4 are present here also. In figure 8 we see that there is almost no emission in the wings and the absorption core has become narrow which again shows that photons are removed from the wings and added to the cores. The above lines have been calculated in a medium in which radiation is scattered both by dust and gas and without any emission.

In figures 9 to 12 we have included thermal emission through the factor $\epsilon = 10^{-4}$ in a static medium. We would like to find out as to how dust scatters radiation when we have thermalization of photons. There is substantial amount of emission on both sides of centre of the line with absorption at the centre. As the amount of dust is increased the two peaks of emission wings are reduced substantially, although there is no change in the width of the central absorption. In figure 12, we have increased the dust optical depth to 5. The emission in the wings completely vanishes. In figures 13 to 16 we have introduced expansion of the medium by giving an expanding velocity of 5 mtu and immediately we see that there is asymmetry in the lines. In figure 13 we see that there are two peaks of emission unequal in heights, the larger one being on the red side of the centre. In figure 14 we see that P-Cygni profile develops. When dust is introduced ($\tau = 0.5$) we notice that

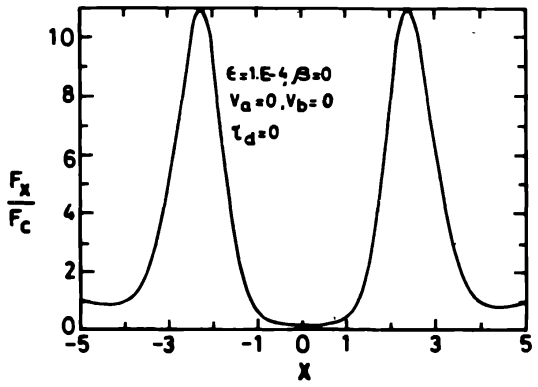

Figure 9. Line profiles formed in a static medium in which there is line emission and no dust included.

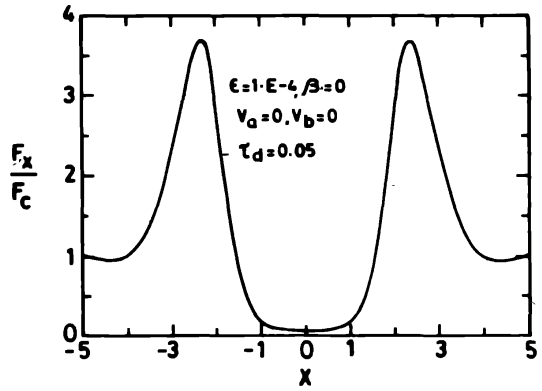

Figure 10. Same as in figure 9 with uniform dust distribution giving a total $\tau_d = 0.05$.

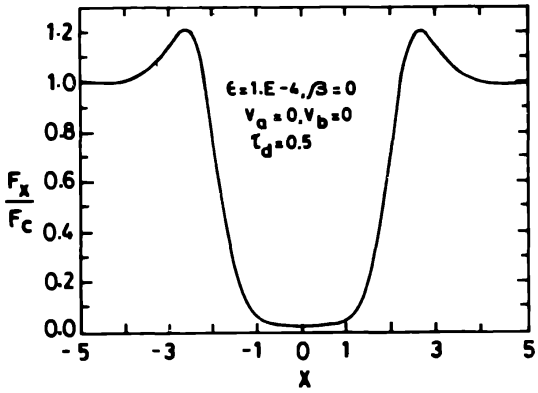

Figure 11. Same as in figure 9 with $\tau_d = 0.05$.

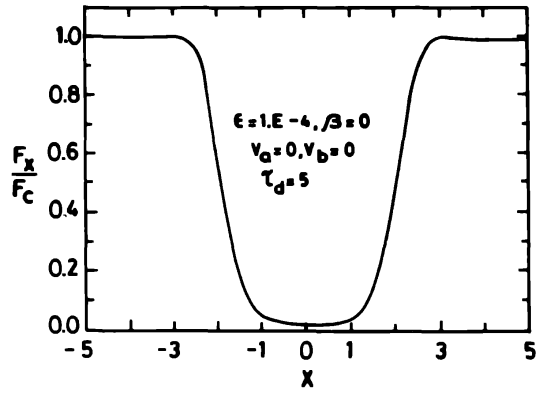

Figure 12. Same as in figure 9 with $\tau_d = 5.0$.

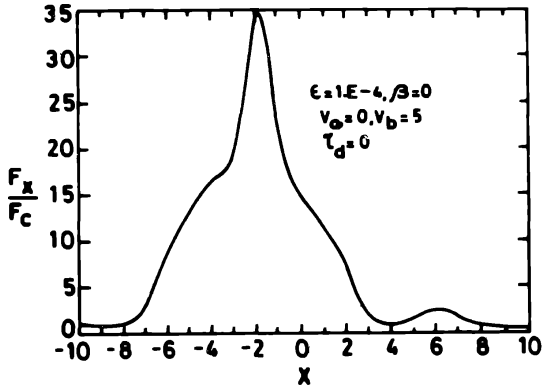

Figure 13. Line profiles formed in an expanding medium with velocity gradients and velocity of expansion $V_b = 5$ mtu, $\tau_d = 0$.

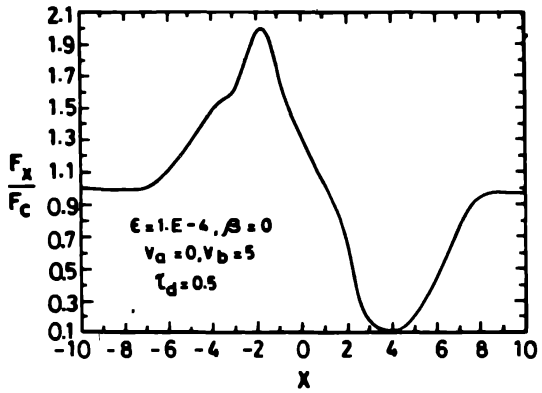

Figure 14. Line profiles formed in an expanding medium with velocity gradients and velocity of expansion $V_b = 5$ mtu, $\tau_d = 0.5$.

there is a substantial decrease in the emission. An absorption core develops and is shifted towards the violet side while the emission remains on the red side of the centre of the line (figure 14). Further increase of dust ($\tau_d = 2$) in figure 15 reduces the emission peak substantially and the absorption core persists. With still further increase in the dust optical depth (figure 16) the absorption core deepens and becomes very dark with hardly any emission in the wings. In figures 17 to 20 the expansion velocity has been increased to 10 mtu and the same behaviour as we find in figures 13 to 16 occurs. In figures 21 to 24 we have plotted the profiles in a shell expanding uniformly which means that there are no velocity gradients, the velocity expansion of the shell being 5 Doppler widths (mtu). In figure 21 the profiles are given for 5 mtu and there are two peaks of emission as in the earlier cases. The emission peak on the red side is larger and flat-topped. When the dust optical depth is increased to 0.05 the emission is reduced considerably although the flat-topped peak remains. In figures 25 to 28 we have increased the expansion velocity to 10 mtu and we see the same behaviour as before.

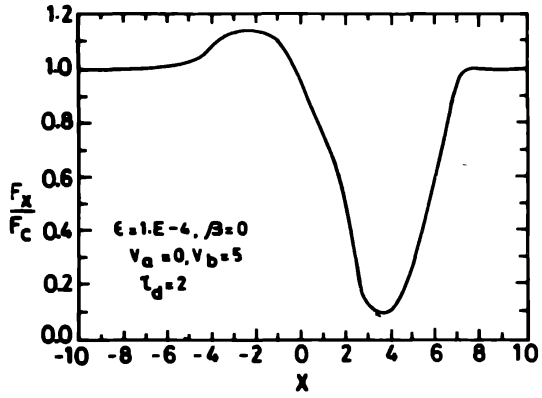

Figure 15. Line profiles formed in an expanding medium with velocity of expansion $V_b = 5$ mtu, $\tau_d = 2.0$.

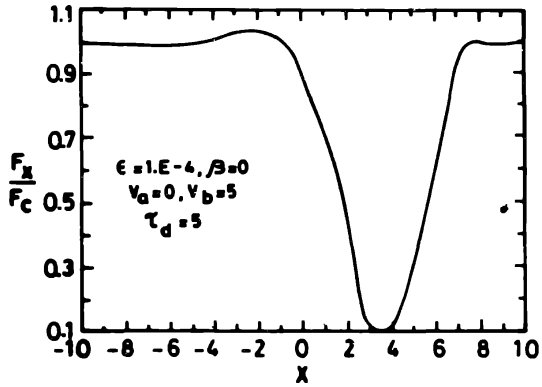

Figure 16. Line profiles formed in an expanding medium with velocity of expansion $V_b = 5$ mtu, $\tau_d = 5.0$.

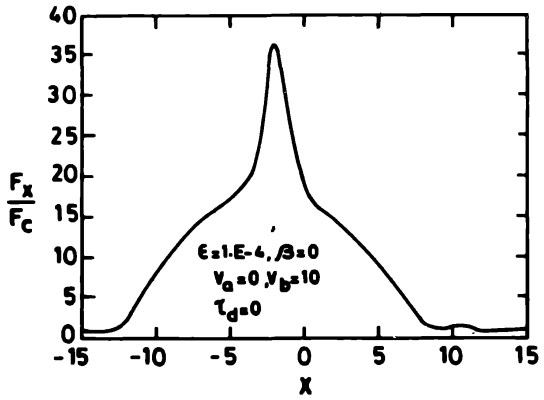

Figure 17. Same as in figure 13 but velocity of expansion is equal to 10 mtu.

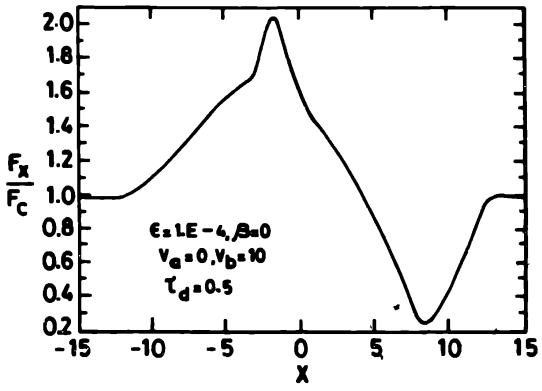

Figure 18. Same as in figure 14 with velocity of expansion $V_b = 10$ mtu.

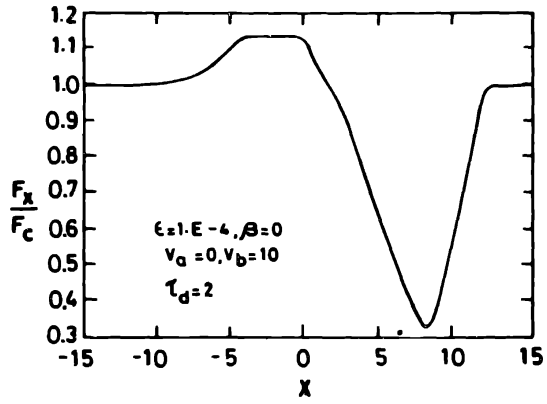

Figure 19. Same as in figure 15 with velocity of expansion $V_b = 10$ mtu.

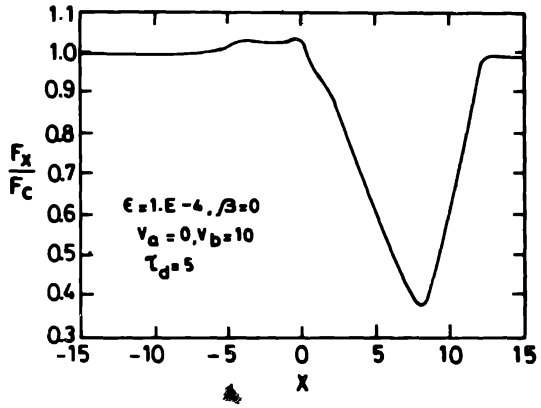

Figure 20. Same as in figure 16 with velocity of expansion $V_b = 10$ mtu.

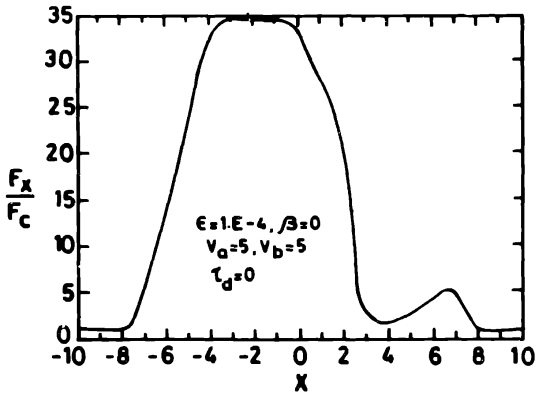

Figure 21. Line profiles formed in an expanding medium without velocity gradients and velocity of expansion $V_b = 5$ mtu, medium containing no dust ($\tau_d = 0$).

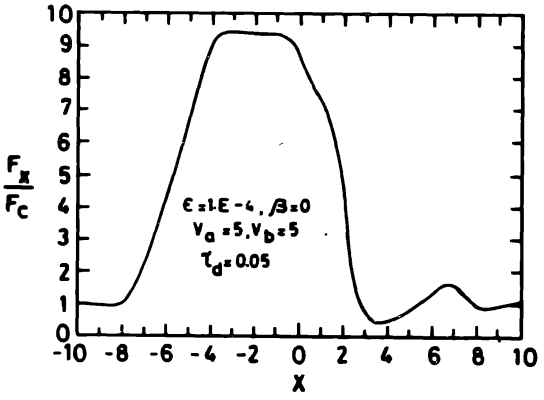

Figure 22. Same as in figure 21 but dust content is given as optical depth $\tau_d = 0.05$.

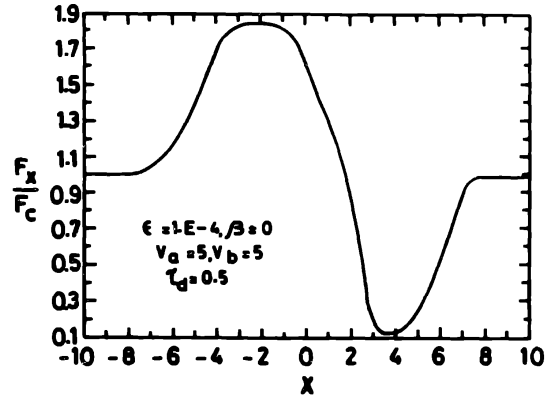

Figure 23. Same as in figure 21 but $\tau_d = 0.5$.

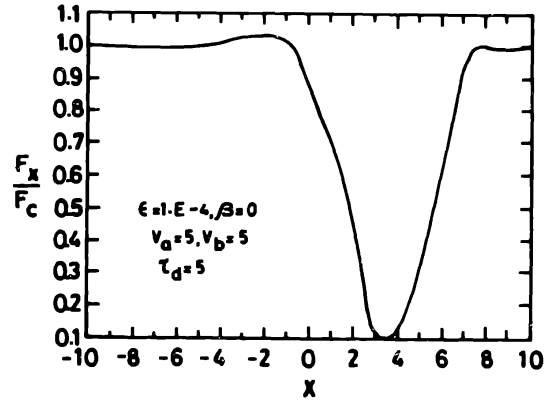

Figure 24. Same as in figure 21 but $\tau_d = 5.0$.

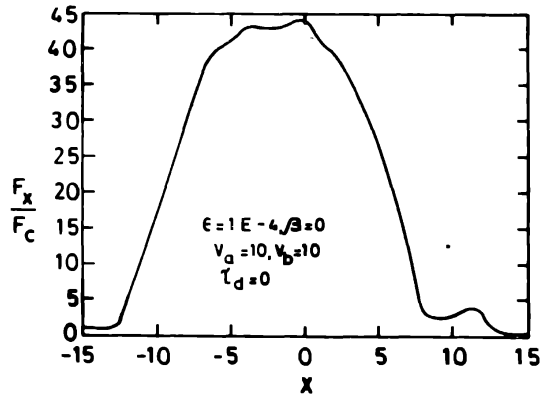

Figure 25. Same as those in figure 21 with velocity of expansion V_b = 10 mtu without dust.

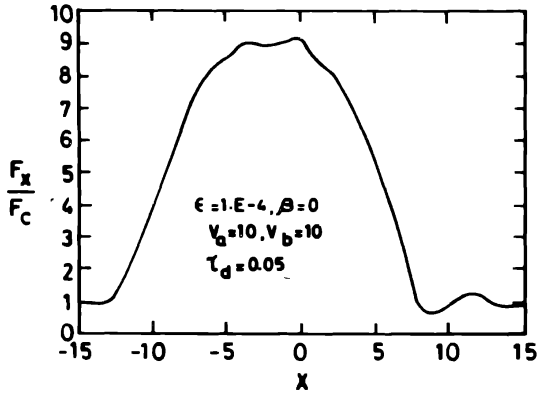

Figure 26. Same as in figure 25 but uniform dust distributed offering an optical depth τ_d = 0.05.

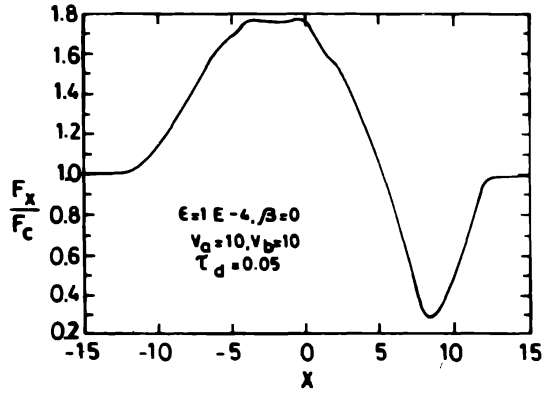

Figure 27. Same as in figure 25 but dust is more, τ_d = 0.5.

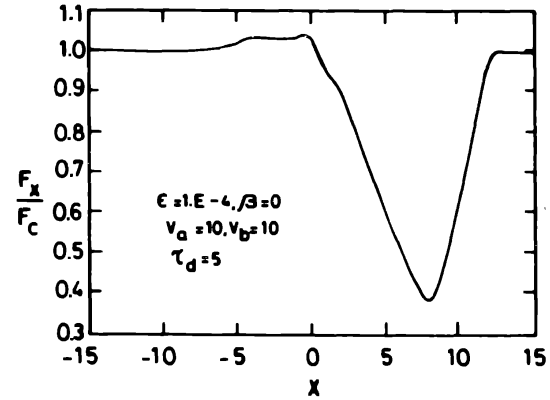

Figure 28. Same as in figure 25 with τ_d = 5.0.

In figures 29 to 44 we have plotted profiles formed in a medium which has continuum emission together with the line emission. They show features similar to figures 9 to 28. In figures 45 and 46 we have plotted the equivalent widths of different lines against different dust optical depth. In figure 45 the equivalent widths correspond to those lines formed in a medium with no velocity gradients while those in figure 46 for a medium expanding with velocity gradients. These results are for a medium which scatters radiation (by both gas and dust). There are large differences in the equivalent widths between the lines formed in media with velocity gradients and those formed in media without velocity gradients. As the dust optical depth increases the equivalent widths in a medium moving with velocity gradients are reduced while the equivalent widths formed in media moving without velocity gradients increase, the emission is considerably reduced. In figures 47, 48 and 49 we have plotted the ratio of heights of the two emission peaks. We see that the ratio falls as the dust optical depth is increased. In figure 50 we have plotted the equivalent widths against the velocity of expansion in a medium which is moving with velocity gradients for two dust optical depths that is, 0 to 2. Now we see that equivalent widths increase as the velocity of expansion increases. In figure 51 we have

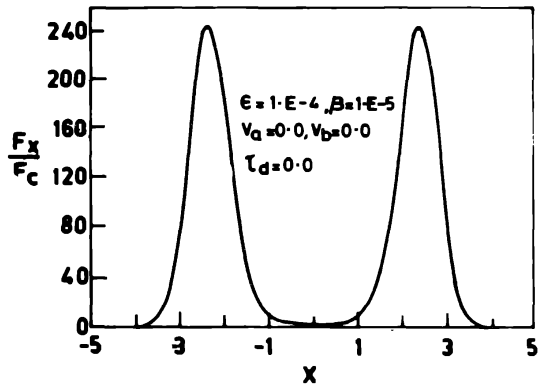

Figure 29. Line profiles in a static medium without dust.

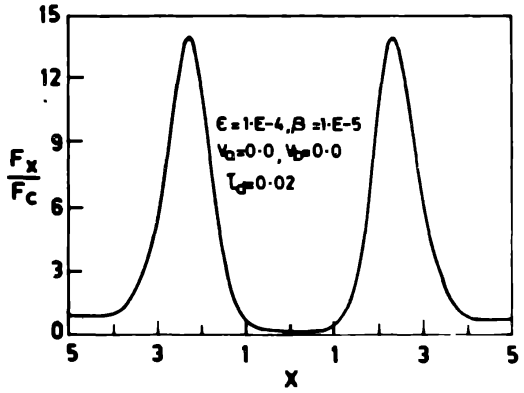

Figure 30. Line profiles formed in a static medium with dust, $\tau_d = 0.02$.

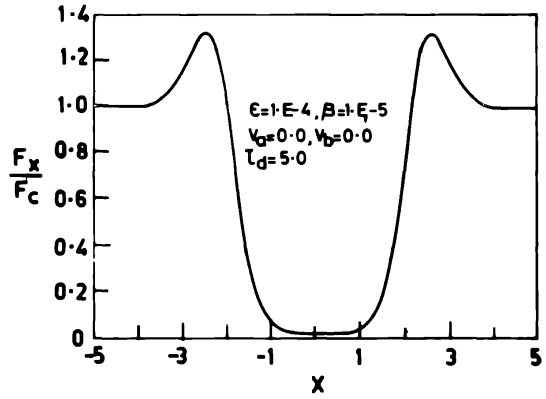

Figure 31. Line profiles formed in a static-medium with dust, $\tau_d = 0.5$.

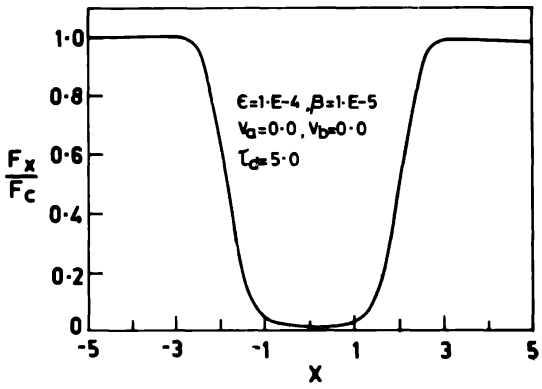

Figure 32. Line profiles formed in a static medium with dust, $\tau_d = 5.0$.

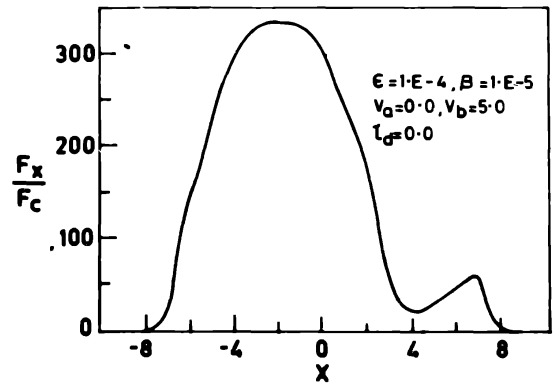

Figure 33. Line profiles formed in an expanding medium with velocity gradients and velocity of expansion $V_b = 5$ mtu.

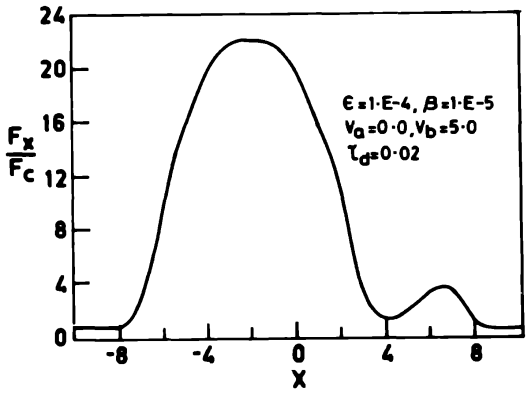

Figure 34. Same as in figure 33, with dust contained in the medium $\tau_d = 0.02$.

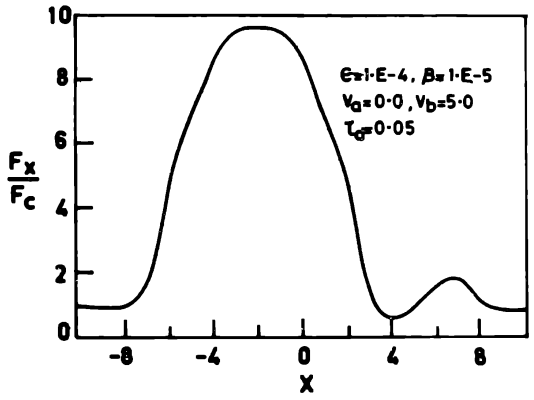

Figure 35. Same as in figure 33, with dust contained in the medium $\tau_d = 0.05$.

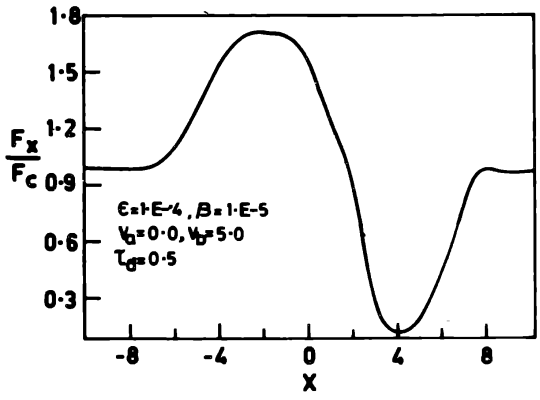

Figure 36. Same as in figure 33, with dust contained in the medium $\tau_d = 0.5$.

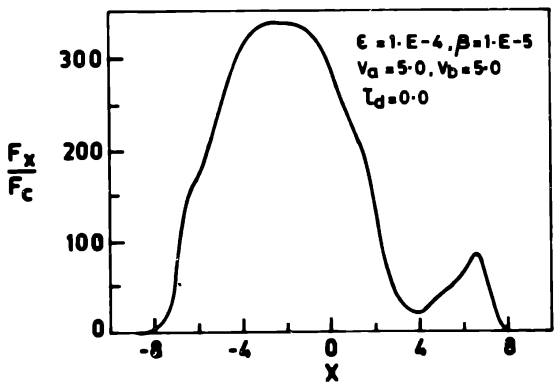

Figure 37. Line profiles formed in an expanding medium without velocity gradients, velocity of expansion is equal to 5 mtu.

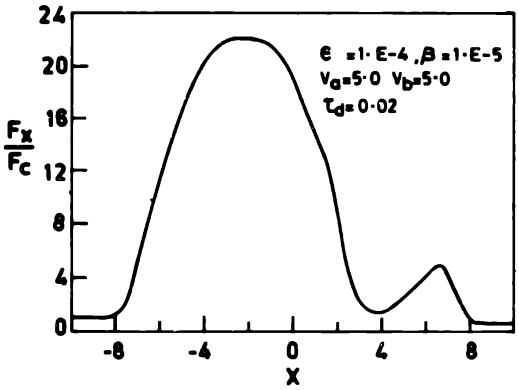

Figure 38. Same as those of figure 37 but with dust $\tau_d = 0.02$.

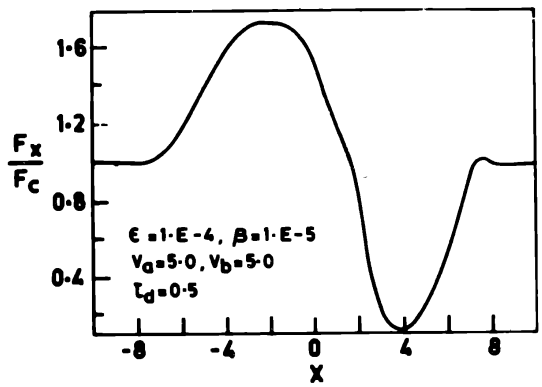

Figure 39. Same as those of figure 37 but with dust $\tau_d = 0.5$.

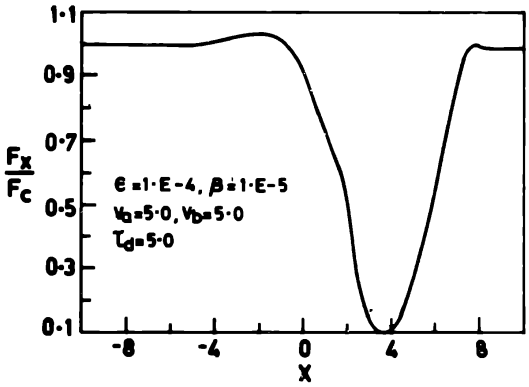

Figure 40. Same as those of figure 37 but with dust $\tau_d = 5.0$.

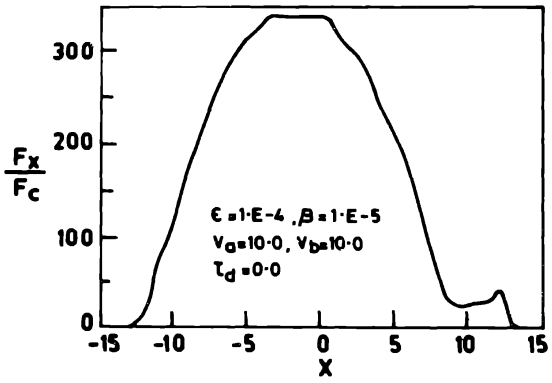

Figure 41. Line profiles formed in an expanding medium without velocity gradients, velocity of expansion of the medium V_b = 10 mtu.

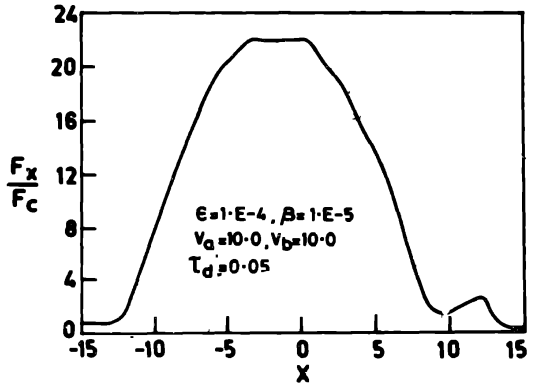

Figure 42. Same as in figure 41 but with dust τ_d = 0.05.

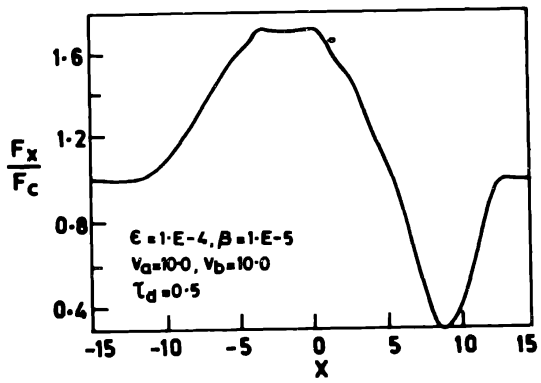

Figure 43. Same as in figure 41 but with dust τ_d = 0.5.

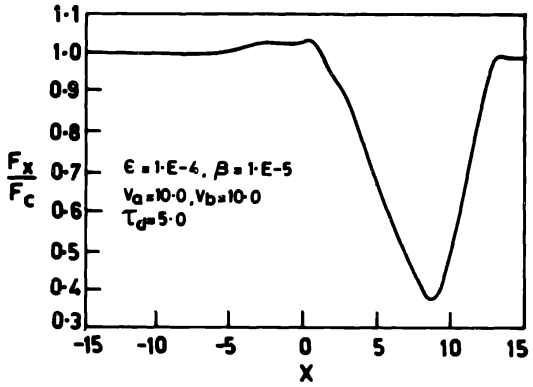

Figure 44. Same as in figure 41 but with dust τ_d = 5.0.

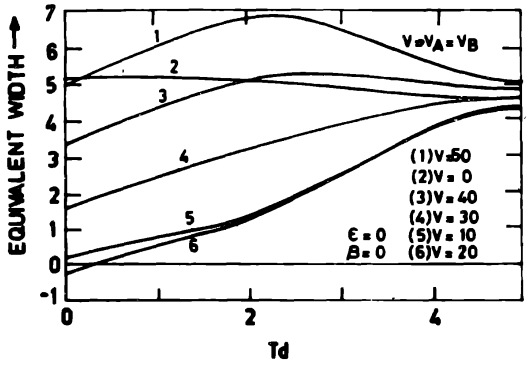

Figure 45. Variation of equivalent widths with dust optical depth (τ_d) for various velocities of expansion (without velocity gradients).

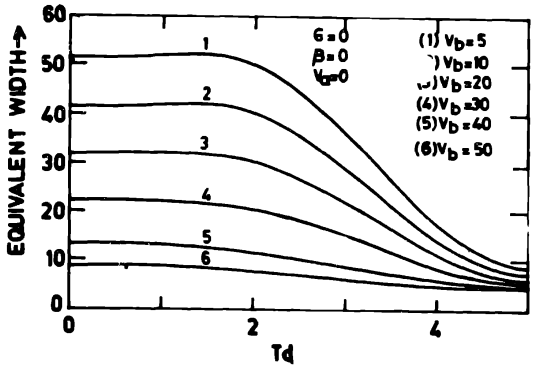

Figure 46. Same as in figure 45 but with velocity gradients.

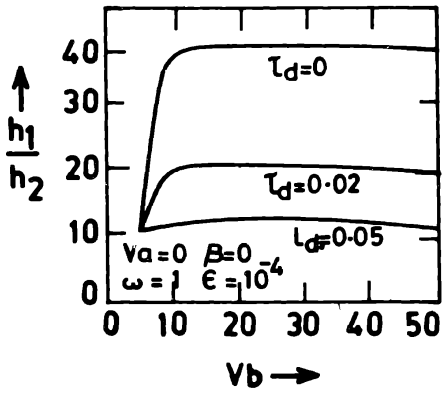

Figure 47. Variation of the ratio of two emission peak heights (h_1/h_2) in an expanding medium with velocity (V_b) (with velocity gradients).

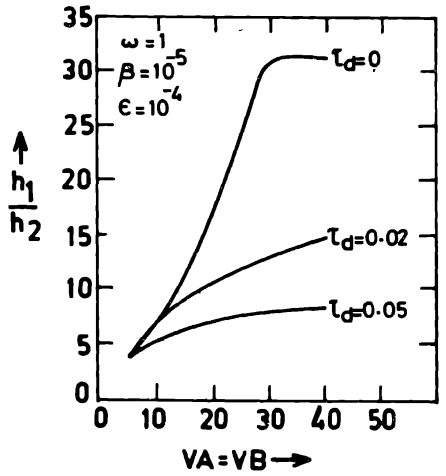

Figure 48. Same as those of figure 47 but without velocity gradients

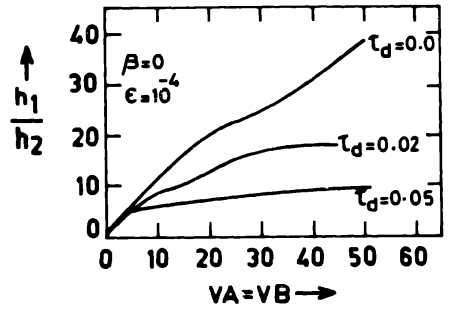

Figure 49. Same as in figure 48 for $\beta = 10^{-5}$.

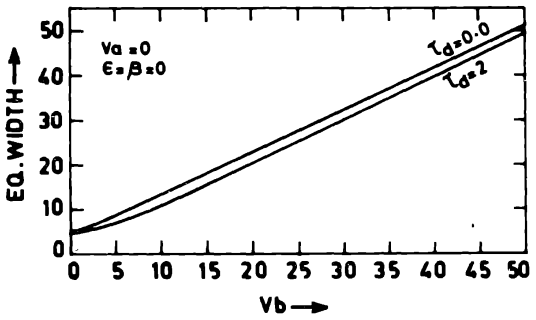

Figure 50. Variation of equivalent width of lines with velocity of expansion (with velocity gradients).

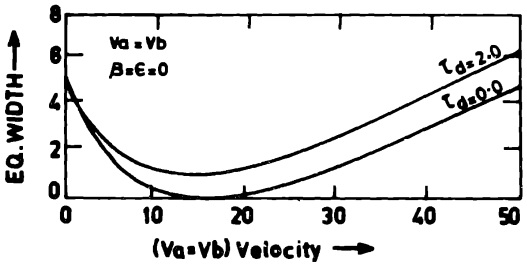

Figure 51. Same as those in figure 50 (without velocity gradients).

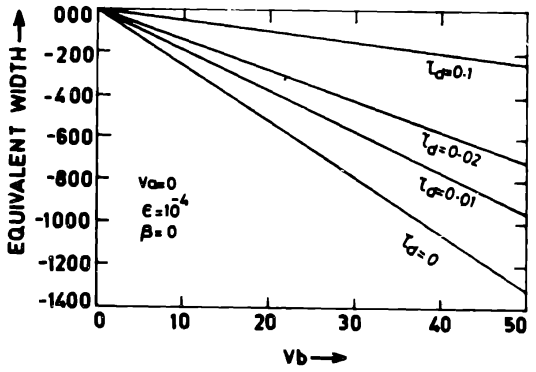

Figure 52. Same as those of figure 50 but for $\epsilon = 10^{-4}$.

shown how the equivalent width changes in a medium which is moving without velocity gradients whereas in the earlier case the equivalent widths increase almost linearly. In the present case the equivalent width falls upto 15 mtu and then a further increase in velocity, increase the equivalent widths.

In figure 52 the equivalent widths are plotted for a medium expanding with velocity gradients and with thermal emission in the line. Here we notice that all the lines are in emission and it is also noticed that the emission reduces as we increase the amount of dust. In figure 53 we have plotted the equivalent widths for a medium without velocity

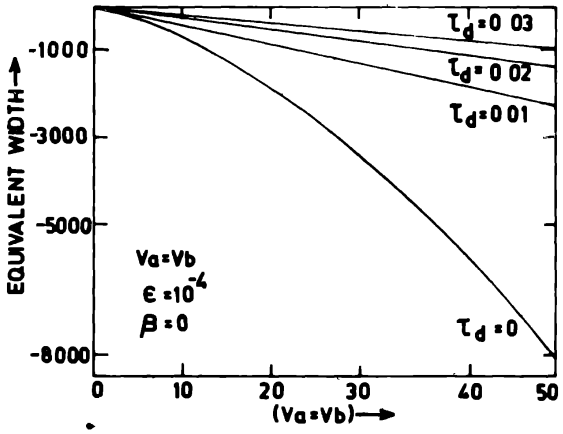

Figure 53. Same as those of figure 51 but for $\epsilon = 10^{-4}$.

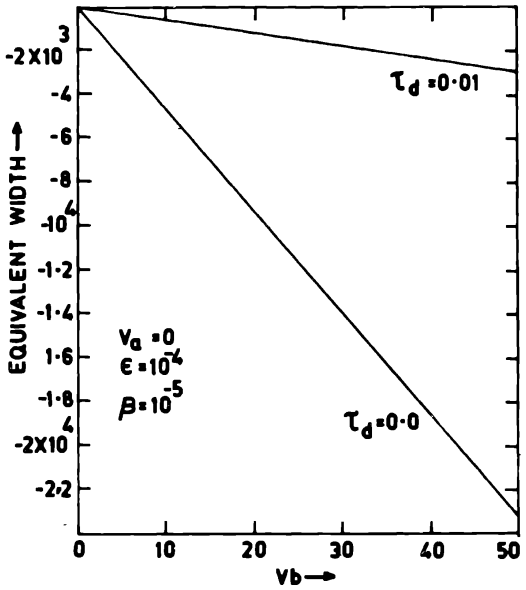

Figure 54. Same as those in figure 50 but with $\epsilon = 10^{-4}$ and $\beta = 10^{-5}$.

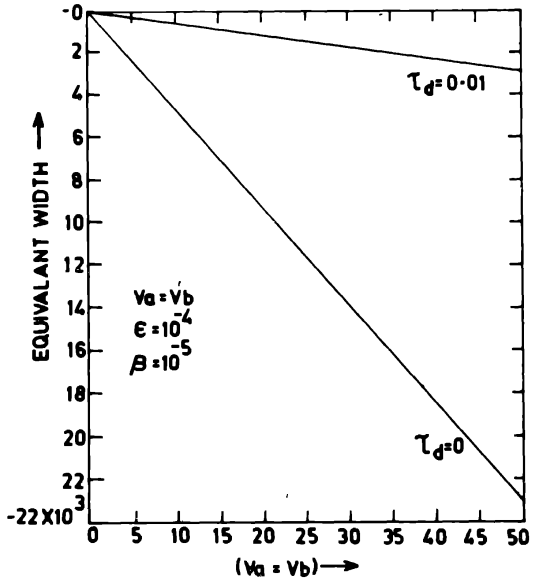

Figure 55. Same as those in figure 51 and $\epsilon = 10^{-4}$ and $\beta = 10^{-5}$.

gradients and the same behaviour of the equivalent widths is noticed as in the previous case. In figures 54 and 55 the equivalent widths are plotted for a medium in which there is emission both in the line and continuum and the behaviour of the equivalent widths is similar to those as in a medium where there is line emission only.

References

Allen, D. A. (1973). *M.N.R.A.S.* **161**, 145.
Allen, D. A. & Swings, J. P. (1972) *Ap. Lett.* **10**, 83.
Chandrasekhar, S. (1945) *Rev. Mod. Phys.* **17**, 138.
Felli, M. (1982) *Mem. Soc. Acad. It.* **53**, 349.
Grant, I. M. & Peraiah, A. (1972) *M.N.R.A.S.* **160**, 239.
Grasdalen, G. L. (1976) *Ap. J. (Lett.)* **205**, L83.
Geisel, S. L. (1970) *Ap. J. (Lett.)* **161**, L105.
Huggins, P. J., Glassgold & Morris, M. (1984) *Ap. J.* **279**, 284.
Henkel, C., Matthews, H. E. & Morris, M. (1983) *Ap. J.* **267**, 184.
Hummer, D. G. & Kunasz, P. B. (1980) *Ap. J.* **236**, 609.
Kunasz, P. & Hummer, D. G. (1974a, b), *M.N.R.A.S.* **166**, 19; 57.
Kwan, J. & Hilli, F. (1977) *Ap. J.* **215**, 781.
Mihalas, D. (1978) *Stellar atmospheres*, 2nd ed, Freeman.
Mihalas, D., Kunasz, P. B. & Hummer, D. G. (1975) *Ap. J.* **202**, 465.
Peraiah, A. (1984) in *Methods in radiative transfer* (ed.: W. Kalkofen) Cambridge, p. 281.
Peraiah, A. & Wehrse, R. (1978) *Astr. Ap.* **70**, 213.
Peraiah, A., Varghese, B. A. & Srinivasa Rao M. (1987), *Astr. Ap. Suppl.* **69**, 345.
Persi, P., Ferrari-Tonilolo, M. & Grasdalen, G. L. (1983) *Ap. J.* **269**, 265.
Simon, M., Felli, M., Cassar, L., Fischer, J. & Massi, M. (1983) *Ap. J.* **266**, 623.
Simon, M., Righini-Cohen, G., Felli, M. & Fisher, J. (1981) *Ap. J.* **244**, 552.
Schwartz, P. R. *et al.* (1983) *Ap. J.* **271**, 625.
Wehrse, R. & Kalkofen, W. (1985) *Astr. Ap.* **147**, 71.
Wehrse, R. & Peraiah, A. (1979) *Astr. Ap.* **71**, 289.